Atmos. Chem. Phys. Discuss., 13, 26489–26527, 2013
www.atmos-chem-phys-discuss.net/13/26489/2013/
doi:10.5194/acpd-13-26489-2013

Atmospheric Chemistry and Physics Discussions

Will the role of intercontinental transport change in a changing climate?

T. Glotfelty[1], Y. Zhang[1], P. Karamchandani[2], and D. G. Streets[3]

[1]Department of Marine, Earth, and Atmospheric Sciences, Campus Box 8208, North Carolina State University, Raleigh, NC 27695, USA
[2]ENVIRON International Corporation, Novato, CA, USA
[3]Decision and Information Sciences Division, Argonne National Laboratory, Argonne, IL, USA

Received: 25 September 2013 – Accepted: 28 September 2013 – Published: 11 October 2013

Correspondence to: Y. Zhang (yang_zhang@ncsu.edu)

Published by Copernicus Publications on behalf of the European Geosciences Union.

Abstract

Intercontinental transport of atmospheric pollution (ITAP) can offset the impact of local emission control efforts, impact human and ecosystem health, and play a role in climate forcing. This study aims to determine the role of ITAP caused by East Asian anthropogenic emissions (EAAEs) under current and future emission and climate scenarios. ITAP from East Asia is enhanced in the future due to faster wind speeds aloft and a stronger low pressure center over Eastern Russia that facilitate enhanced westerly export in the free troposphere and stronger southerly transport near the surface, increased gaseous precursor emissions, and increased temperatures. As a result, the contribution of ozone (O_3) generated by EAAEs to the global average O_3 mixing ratio increases by ~0.8 ppb from 1.2 ppb in 2001 to 2.0 ppb in 2050. The contribution of $PM_{2.5}$ generated by EAAEs to the global $PM_{2.5}$ level increases by ~0.07 $\mu g\,m^{-3}$ from 0.32 $\mu g\,m^{-3}$ in 2001 to 0.39 $\mu g\,m^{-3}$ in 2050, despite a non-homogenous response in $PM_{2.5}$ resulting from cloud and radiative feedbacks. EAAEs can increase East Asian biogenic secondary organic aerosol by 10–81 %, indicating that it is largely controllable. EAAEs also increase the deposition of nitrogen, black carbon, and mercury both locally and downwind, implying that they may play a role in climate feedbacks and ecosystem health of these regions. These results show that EAAEs have a large impact on global air quality and climate, especially on downwind regions. Such impacts may be enhanced under future climate and emission scenarios, demonstrating a need to synergize global pollution control and climate mitigation efforts.

1 Introduction

Intercontinental transport of atmospheric pollution (ITAP) is of major concern as it can offset the impact of local emission control efforts in certain regions (Jacob et al., 1999; Lin et. al., 2008; Wang et al., 2009, 2012). ITAP of fine aerosols has also been shown to be a health hazard resulting in an estimated 90 000 premature deaths globally in 2000

ACPD
13, 26489–26527, 2013

(Liu et al., 2009). ITAP plays a large role in the Northern Hemisphere (NH), as this is the most populated part of the globe, with three major industrial centers including East Asia, North America, and Europe. East Asia is the most important source region as its lower latitudes and thus higher surface radiation and vertical transport make it more suitable for local ozone (O_3) photochemical production and transport (Bey et al., 2001; Wild and Akimoto, 2001; Stohl et al., 2002). As a result, the Asian free troposphere has been shown to have a large global impact on the seasonal variations and vertical structure of O_3 throughout the troposphere (Sudo and Akimoto, 2007). North America is also an important source to global pollution but it is the most affected receptor to Asian emissions and to a lesser extent by European emissions (Wild and Akimoto, 2001; Fiore et al., 2009). Europe is typically the weakest source region, as weaker convection and the dominance of high pressure systems in summer make horizontal boundary layer advection the primary transport mechanism and this type of transport is typically blocked by the Eurasian terrain and the pollutants are subject to greater local deposition, but transport to the Arctic makes Europe the most important contributor to Arctic haze especially in winter (Wild and Akimoto, 2001; Stohl et al., 2002). Additionally, Europe is a receptor since East Asia has a large global impact (Wild and Akimoto, 2001).

Transport from East Asia to North America occurs primarily through uplifting associated with the warm conveyor belt of mid-latitude cyclones, which lofts the pollutants into the lower free troposphere (FT) where they are transported by westerly winds (Bey et al., 2001; Husar et al., 2001; Hess et al., 2003; Jaffe et al., 2003; Liu et al., 2003; Cooper et al., 2004; Wang et al., 2009, 2012). Additional transport pathways include planetary boundary layer (PBL) outflow behind cold fronts (Liu et al., 2003; Wang et al., 2009, 2012), orographic uplifting in China (Liu et al., 2003), and strong convection (Liu et al., 2003; Takigawa et al., 2005). This uplift is usually associated with fast transport that can occur in as quickly as six days (Jaffe et al., 1999, 2003) Intercontinental transport from North America to Europe has not only been linked to uplift from warm conveyor belts, but also to pyro-convection from wild fires (Ravetta et al., 2008). Wang

ACPD
13, 26489–26527, 2013

et al. (2009) showed that certain pollutants such as CO, O_3, $PM_{2.5}$, and SO_4^{2-} favor transport in both the PBL and lower FT, while other pollutants such as PAN, SO_2, and NO_3^- primarily transport in the lower FT. Wang et al. (2012) showed that dust particles transport at altitudes above 5 km.

Although it may be counter-intuitive, ITAP plays a much larger role in the boreal spring and autumn months as compared to the summer when production of pollutants such as O_3 are higher (Wild and Akimoto, 2001; Shindell et al., 2008; Fiore et al., 2009; Jonson et al., 2010). This is because although convective uplift is greater in the summer, there is more stagnation and thus less significant horizontal transport. Additionally, the lifetime of O_3 is relatively shorter in the summer months due to the additional water vapor resulting from greater evaporation. This occurs because (1) there is a greater chance for $O(^1D)$ to react with H_2O to form OH rather than O which reduces O_3 production, and (2) the increased OH or HO_2 from this process can react remove O_3 directly. Thus, transport is most effective in spring as the frequency of uplift from mid-latitude cyclones is high and the westerly transport is more direct (Wild and Akimoto, 2001). However, it can still play a minor role in the summer, e.g., it accounts for 3 % of the North American O_3 budget (Pfister et al., 2008).

The Task Force on Hemispheric Transport of Air Pollution (HTAP) was formed in 2004 to improve the understanding of ITAP in the NH. The HTAP program included a multi-model ensemble of experiments that compared the impact of 20 % reductions in anthropogenic emissions from their baseline levels in the four largest industrial centers including Europe, North America, East Asia, and South Asia. The aim of these multi-model ensemble experiments was to estimate the sensitivity of each region's ambient pollution to these emission reductions. These studies, along with others were compiled into the 2010 Task Force on Hemispheric Transport of Air Pollution report (TF-HTAP) (http://www.htap.org/). These experiments found that during spring months the 20 % emissions reductions largely from Asia can reduce the ozone level over 1 ppb or greater at Trinidad Head, CA at the surface and throughout the troposphere (Jonson et al., 2010). These reductions in East Asia emissions typically result in a decrease in the

ACPD
13, 26489–26527, 2013

maximum 8 h O_3 mixing ratio (max 8 h O_3) by ~0.9 ppb regardless of its level in the Western US, but its magnitude of decrease varies with the max 8 h O_3 level in the Eastern US (e.g., decreasing by 0.65 and 0.3 ppb at lower and higher max 8 h O_3, respectively) (Reidmiller et al., 2009). The emission reductions of O_3 precursors from East Asia were estimated to decrease the annual mortality rate in North America by 200 deaths but could decrease the number of premature deaths by as much as 5900 over the entire NH (Anenberg et al., 2009). The experiments also revealed that long-term responses to surface ozone from emissions reductions of CH_4 is as large as the impact from reducing emissions of nitrogen oxides (NO_x), total non-methane volatile organic compounds (VOC), and CO combined (Fiore et al., 2009). A subset of the HTAP models reveals that projected climate change increases the impact of reducing anthropogenic emissions in source regions but reduces the impact on receptor regions (Doherty et al., 2013). In addition to the impacts on O_3, these emissions reductions have been shown to decrease the reactive nitrogen deposition in North America by 1.3 % (Sanderson et al., 2008). The HTAP modeling also showed that East Asia contributes 19 %, 31 %, 29 %, and 28 % to the Arctic sulfate, black carbon (BC), CO, and O_3, respectively during the spring months. During the summer months when the BC snow albedo feedback is the strongest, BC deposition from East Asia is important and comparable to that from North America (Shindell et al., 2008).

Other studies have also investigated the impact of long range transport of East Asian aerosols (Park et al., 2004; Hadley et al., 2007; Koch et al., 2007; Liu et al., 2008; Yu et al., 2008; Leibensperger et al., 2011). It is estimated that 4.4 $Tg\,a^{-1}$ of fine aerosol pollution is imported to North America from Asia, which is equivalent to approximately 15 % of local emissions (Yu et al., 2008). This transport contributes 10–30 % and 30–50 % to the background sulfate over the Eastern and Western US, respectively, and 75 % to the BC over North America (Park et al., 2004; Hadley et al., 2007; Liu et al., 2008). Emissions of other compounds such as NO_x and CO in East Asia have also been shown to increase the concentrations of fine particles ($PM_{2.5}$) by 1.0 $\mu g\,m^{-3}$ in the Eastern US (Leibensperger et al., 2011). Additionally, aerosols emitted from East Asia

ACPD
13, 26489–26527, 2013

can have several climatic impacts (Lau et al., 2006a, b; Menon et al., 2002; Roberts et al., 2006; Qian et al., 2003, 2006, 2007; Zhang et al., 2007). Compared to ultrafine marine aerosols, long range transport of anthropogenic particles in stratified layers from 1000–7000 m above the surface of the Eastern Pacific have been shown to play a more important role in the aerosol direct and indirect effects as their larger size increases their likelihood of activation and thus effectiveness of scatter radiation (Roberts et al., 2006). Light absorbing aerosols have been linked to the enhancement of winter time convection over the North Pacific (Zhang et al., 2007) and to dynamic and thermodynamic feedbacks that can alter the Asian monsoon (Lau et al., 2006a, b). The light absorbing BC aerosols emitted in East Asia have also been shown to result in dimming of 1.45–1.47 $W m^{-2}$ in the Western US (Hadley et al., 2007). In China, increasing aerosol emissions provides a plausible explanation for the decreasing solar radiation reaching the surface despite decreasing cloud cover (Qian et al., 2003, 2006, 2007). It has also been shown that areas with high anthropogenic emissions, such as East Asia, can contribute substantially to the formation of local biogenic secondary organic aerosol (BSOA) (Carlton et al., 2010 and references therein).

This study aims to determine the role of the ITAP from East Asian anthropogenic emissions (EAAEs) in global air quality and climate under current and future emissions and climate scenarios. Specifically, several science and policy-related questions will be addressed. For example, how will the role of ITAP change under future scenarios? What processes and factors will dominate such changes? How much BSOA can be reduced through reducing EAAEs? Such information would be very useful to guide the development of future emission control and climate mitigation strategies in a changing climate.

2 Experimental design

The model used in this work is the newly developed Global-through-Urban Weather Research and Forecasting Model with Chemistry (GU-WRF/Chem) of Zhang et al.

ACPD
13, 26489–26527, 2013

(2012b). This model is an online-coupled meteorology and chemistry model, which enables the simulation of the climate feedbacks associated with aerosols and radiative gases from global to urban scales. It was developed by first replacing the WRF model in the National Oceanic and Atmospheric Association (NOAA)'s mesoscale WRF/Chem with the National Center for Atmospheric Research (NCAR)'s global WRF (GWRF) and then improving several model treatments for their applications on hemispheric to global scales including online dust and biogenic volatile organic compounds (BVOCs) emissions, gas-phase chemistry, a photolytic rate scheme, aerosol chemistry and microphysics, and aerosol-cloud interactions. GWRF and GU-WRF/Chem have been evaluated using meteorological, radiative, and chemical observations from surface networks and satellites. They demonstrate satisfactory performance as compared to other existing global and mesoscale atmospheric models (Zhang et al., 2012a, b).

GU-WRF/Chem simulations are first completed for the full years of 2001, 2010, 2020, 2030, 2040, and 2050 to characterize the trends of climate changes based on an average of current years (AOC), consisting of the years 2001 and 2010 and an average future time period (AOF) consisting of the years 2020, 2030, 2040, and 2050. These results will be presented in a separate paper. In this work, the boreal spring months (March, April, and May (MAM)) during 2001 and 2050 during which ITAP is the strongest for the Trans-Pacific region are selected to study the role of intercontinental transport of East Asian air pollutants and their impacts on the US and global air quality and climate. Additional simulations under different emission and climate scenarios for MAM 2001 and 2050 are conducted and compared to those of the MAM 2001 and 2050 simulations as part of the aforementioned multi-year simulations. The suite of model simulations conducted includes three baseline simulations with EAAEs during MAM: 2001 with current climate conditions and emissions, 2050 with projected climate change and emissions, and 2050 with projected climate change only (referred to as 2001, 2050, and 2050_CCO, respectively), and three sensitivity simulations in which EAAEs are removed in the East Asia region including China, North and South Korea, Japan, and portions of India, Mongolia, Southeast Asia, and Russia. Unlike the

ACPD
13, 26489–26527, 2013

20 % reductions of anthropogenic emissions used in HTAP, all Asian anthropogenic emissions are zeroed out in the sensitivity simulations in this work to estimate the maximum possible impacts of EAAEs on global air quality and climate. The anthropogenic emission inventory used for the 2001 simulations is described in Zhang et al. (2012b) and the 2050 emissions are generated using regionwide growth factors based on the Intergovernmental Panel on Climate Change Special Report on Emissions version 4 A1B scenario. The growth factors are developed following the approach of Nakicenovic et al. (2000) and RIVM (2001) and are provided in the Supplement. Natural emissions of BVOCs, dust, and sea-salt are calculated online using the Model of Emissions of Gases and Aerosols from Nature version 2 (MEGAN2) (Guenther et al., 2006), the dust scheme of Shaw (2008) with the modifications of Zhang et al. (2012b), and the sea salt scheme of Gong et al. (1997) with an updated treatment for smaller sea-salt particles from O'Dowd et al. (1997), respectively. The initial conditions for meteorological variables and some chemical species such as CH_4, N_2O, and O_3 in all simulations are generated from the Community Climate System Model version 3 (CCSM3) SRESA1B data set. Initial conditions for additional species not available from CCSM outputs (e.g., PAN, H_2O_2, and SO_2) are generated from the Goddard Earth Observing System Model with Chemistry v7-04-12-Run0 (GEOS-Chem). The initial conditions obtained from CCSM3 are decadal mean values to reduce interannual variability in the simulations, thus the 2050 simulation is initiated by the average of CCSM3 output for the period of 2045–2054. 2001 was initialized by the average of CCSM3 output from only the five year period 2000–2004 due to lack of data during 1995–1999. The initialization of species from GEOS-Chem data was based on monthly mean values. Since future GEOS-Chem simulations were not available, all years are initialized using the same dataset as that for 2001. A one month spin-up period is used to bring all chemical species into equilibrium with the new emissions and provide initial conditions for missing species. The meteorological fields are reinitialized every month from CCSM3 and the chemical species are initialized based on the previous month's simulation. A more detailed description of model configurations can be found in Zhang et al. (2012b).

ACPD
13, 26489–26527, 2013

3 Representativeness of 2001 and 2050

The simulation results in 2001 and 2050 are first compared with the averages of AOC and AOF, respectively, to determine their representativeness as a typical year for current-year and future-year climatology. The predictions of GU-WRF/Chem are also compared with those from an established climate model, i.e., the NCAR's CCSM to demonstrate its skills in simulating current and future climate. Figure 1 compares the average MAM 2 m temperature (T2), 2 m water vapor mixing ratio (Q2), precipitation rate (PR), and planetary boundary layer height (PBLH) for the GU-WRF/Chem 2001 and AOC simulations and CCSM3 initial conditions (2000–2014). Similar plots for 2050 are shown in Fig. 2 in contrast to the AOF from GU-WRF/Chem and CCSM3 initial conditions (2015–2055).

In general, the 2001 and 2050 simulations have the same general spatial pattern as the AOC and AOF from GU-WRF/Chem, respectively. The global average T2 in 2001 and 2050 is 0.09 °C and 0.5 °C larger than the AOC and AOF values, respectively, while the values are ~4.0 °C warmer than the CCSM3 current and future periods. The discrepancy between GU-WRF/Chem and CCSM3 most likely results from a warm bias of ~4.0 °C against National Climatic Data Center (NCDC) global observations. The differences between the individual years of 2001 and 2050 and longer term average AOF and AOC are smaller than the differences between the average current and future periods (1.37 °C warming between 2050 and 2001, 0.79 °C warming between AOF and AOC, and 1.46 °C warming between CCSM3 AOF and CCSM3 AOC), indicating that the differences in T2 between the subset period, i.e., 2050 and 2001 are representative of the average climate change between future and current years. The global average Q2 is 0.09 $g\,kg^{-1}$ less in 2001 than AOC and 0.02 $g\,kg^{-1}$ more in 2050 than AOF. The differences against CCSM3 are much higher (0.72 $g\,kg^{-1}$ between 2001 and CCSM AOC and 0.84 $g\,kg^{-1}$ between 2050 and CCSM AOF), which may be due to an over-prediction of ~0.5 $g\,kg^{-1}$ in the GU-WRF/Chem baseline simulation. Similarly to T2, the climate change signal between the current and future simulations (i.e., 0.67 $g\,kg^{-1}$

ACPD
13, 26489–26527, 2013

increase between 2050 and 2001, 0.37 g kg^{-1} increase between AOF and AOC, and a 0.55 g kg^{-1} increase between CCSM3 AOF and CCSM3 AOC) is larger than the discrepancies between the single years and the longer term average AOF and AOC of GU-WRF/Chem simulations.

GU-WRF/Chem does not produce a strong climate signal for PR with only small increases of 0.02 mm day^{-1} between 2001 and 2050 and 0.01 mm day^{-1} between AOF and AOC. For comparison, the increase in PR between CCSM3 AOF and CCSM3 AOC is 0.08 mm day^{-1}. The differences in climate change singal in PR between the two models are mainly due to differences in the cumulus and resolved cloud schemes. These differences are similar in magnitude to the discrepancies between 2001 and AOC (0.01 mm day^{-1}) and 2050 and AOF (0.02 mm day^{-1}), indicating that differences in this parameter cannot clearly be differentiated from internal model variability. Changes in the PBLH between the CCSM3 output and GU-WRF/Chem are quite large. There is a trend of decreasing PBLH in GU-WRF/Chem with global average decreases of 29 m between 2001 and 2050 and 15 m between AOF and AOC, whereas the changes in PBLH are insignificant between CCSM3 AOF and AOC (with an increase of 1 m). This discrepancy in climate change signal in PBLH between models is due to differences in the PBL parameterizations used different models (Murazaki and Hessm, 2006). However, the climate change signal is much larger than the variability between years (4 m between 2001 and AOC and 8 m between 2050 and AOF).

Although some differences between climate change signals obtained using single year differences (i.e., 2050–2001) vs. multi-year average differences (i.e., averages of 2020, 2030, 2040, and 2050 minus averages of 2001 and 2010) due to interannual variability, the above comparison suggests that the differences in meteorology and subsequently chemistry between the 2001 and 2050 simulations are generally representative of a climate change signal obtained using multi-year averages of GU-WRF/Chem simulations. The climate change signals from both the subset of years and the GU-WRF/Chem averages for temperature and humidity are comparable to those from CCSM3, demonstrating the skills of GU-WRF/Chem in simulating current and fu-

ACPD
13, 26489–26527, 2013

ture climate. Some differences exist for PR and PBLH simulated by the two models, mainly because they are more sensitive to the individual models' physical parameterizations (i.e., cumulus/resolved cloud and PBL schemes) than temperature and water vapor.

4 Changes in future emissions

Figure 3 shows the logarithm of the effective growth factors for the 2050 emissions vs. the 2001 baseline emissions. The anthropogenic emissions of O_3 precursors, NO_x and VOCs, increase over most of the globe, with the exception of the US, Canada, Western Europe, Australia, and portions of Northern Asia, leading to global average increases by 38 % and 23 %, respectively, according to the A1B scenario. The East Asian region NO_x increases by ~25–300 % and VOC increases by ~25–150 %, indicating a potential forincreased O_3 and peroxyacetyl nitrate (PAN) production in East Asia. Anthropogenic CO emissions decrease by ~11 % on global average. Developed regions in North America, Australia, Europe, and Northern Asia show the largest declines (~20–97 %), while developing regions in Africa, South America, and South Asia experience increasing emissions (25–280 %). The impact of these emissions on total East Asian CO emissions is uncertain, as the decrease over China and increases over South East Asia are similar (< 25 %) and there are increases in biogenic emissions over Southeast Asia and Northeastern China (Figure not shown) that may have some impacts (10–30 %).

The trends vary in anthropogenic emissions of fine particulate matter ($PM_{2.5}$) precursors and primary anthropogenic emissions. SO_2 emission reductions over the Northern Hemisphere vary from smaller decreases (< 20 %) in China, Japan, and the US to larger decreases (60–92 %) in Europe and Northern Asia. These decreases are compensated by large increases (99–1500 %) in South Asia, South America, and Africa, leading to a global average increase by 20 %. The trend is slightly different for NH_3 emissions (not shown) with decreases by less than 20 % in the conterminous US, 20–

ACPD
13, 26489–26527, 2013

37 % in China, and 50–83 % in Europe and increases by 25–99 % in Mexico, Northern Asia, and South America and larger increases in Africa of up to 195 %. Black carbon (BC) emissions are reduced largely in the US, Canada, Japan, Western Africa, and Western Europe (20–60 %) with smaller decreases in China (< 20 %) and increases over the remainder of the globe. Emissions of primary organic aerosol (POM) largely decrease by 20–75 % over much of globe, with the exception of Northern Asia, North Africa, Australia, and portions of South America, leading to a global average decrease by ∼19 %. These emission changes give no clear insight into the possible changes in East Asian $PM_{2.5}$ as changes over Southeast Asia are typically opposite to those over China and Japan. Overall, North America, with the exception of Mexico, will experience a decline in local anthropogenic emissions by 2050 based on the A1B scenario. Thus, increases in ambient concentrations of pollutants in NA could be attributed to enhanced transport from other regions, enhanced natural emissions, or enhancements from climate change.

The SRES A1B emissions used in this study are not directly comparable to any of the current IPCC regional concentration pathway (RCP) emission scenarios. The moderate RCP pathway with a stabilization of anthropogenic radiative forcing at 6 $W m^{-2}$ by 2100 (RCP6.0) is an updated version of the SRES B2 scenario which is more optimistic scenario than A1B (Masui et al., 2011). The most pessimistic RCP scenario with a stabilization of anthropogenic radiative forcing at 8.5 $W m^{-2}$ by 2100 (RCP8.5) is an updated version of the SRES A2 scenario, which is considered a relatively more pessimistic scenario as compared to A1B (Riahi et al., 2011). The RCP6 scenario includes emission reductions over much of the globe but increases in emissions of all the aforementioned species in China and some portions of Africa, which does support a more optimistic scenario than A1B. The RCP8.5 scenario more closely matches with the A1B scenario, especially in East Asia and North America, where emissions of NO_x and VOCs largely increase and emissions of BC and POM largely decrease over most of East Asia, and emissions of most speciesexcept for NH_3 decrease in North America. The RCP8.5 East Asian CO and SO_2 emissions are similar to A1B with a few

ACPD
13, 26489–26527, 2013

differences. CO emissions in China decrease slightly but, unlike A1B, the Southeast Asia emissions also decrease. The SO_2 emissions decrease to a much larger extent in Eastern China under RCP8.5 but increase similarly to A1B in South and Southeast Asia. Among all emitted species, the trends in NH_3 emissions differ the most as A1B indicates decreases in both North America and East Asia, whereas RCP8.5 increases emissions in both regions.

5 Impact of EAAEs on current and future air quality

The predicted flow patterns at 10 m and 5500 m and the sea level pressure for 2001, 2050, AOC, and AOF are shown in Fig. 4, which illustrates two major pathways of ITAP for East Asia. At the surface, there is both a northerly track that exports pollutants to the Arctic and a stronger westerly track that transports the pollution over the Pacific Ocean to Western North America. The key feature generating this transport is an average anticyclone centered over the East China Sea that exports pollution from East Asia to the north and east. This is similar to the findings reported in Zhang et al. (2008), which indicated a northern transport pathway that is associated with circulation around the Aleutian low and a southern branch responsible for transport to North America associated with circulation around the Pacific high. These two transport pathways were considered to be representative of Trans-Pacific transport climatology (Zhang et al., 2008). In general, the surface pressure patterns are similar among all scenarios with a few key exceptions. In 2050, 2050_CCO (figure not shown), and AOF a stronger low pressure center exists over Eastern Russia than in 2001 or AOC, which results in enhanced transport to the Arctic. Additionally, the average low pressure system over the North Atlantic lifts to the north and east (to a lesser extent in AOF than 2050) which removes the stagnant (i.e., low wind speed) conditions over Northern Europe and Scandinavia in 2001 and AOC. In the free troposphere, transport is primarily westerly. Simulated wind speeds aloft increase over East Asia and decrease over Southern North America in both 2050, 2050_CCO, and AOF. This increases the westerly export

ACPD
13, 26489–26527, 2013

of pollutants lofted into the free troposphere from East Asia, while simultaneously increasing the lifetime of these pollutants over North America, and thus increases the likelihood of subsidence to the surface in the receptor regions.

Figure 5 shows the differences in max 8 h O_3 mixing ratio and the differences in the 24° N to 60° N meridional averaged vertical profiles of O_3 between the simulations with and without EAAEs for 2001, 2050, and 2050_CCO. In 2001, O_3 generated by EAAEs contributes 1.2 ppb to the max 8 h O_3 on a global average, with higher values in several regions (e.g., 3–33.5 ppb in East Asia, 1–2 ppb in Western North America, and 1–3 ppb in the Arctic). In 2050, this contribution increases to ~2 ppb of max 8 h O_3 on a global average, and in several regions (e.g., 4–44.6 ppb in East Asia and 2–5 ppb in Western North America and the Arctic). This is primarily a result of projected increases in East Asian emissions of O_3 precursors in the future, with some regional enhancement from climate change. The 2050_CCO simulations have the same contribution of 1.2 ppb on global average as 2001, but a somewhat different pattern in regional contributions (e.g., 3–37.7 ppb in East Asia, 1–3 ppb in Western North America and the Arctic). The differences in O_3 between the 2001 and 2050_CCO simulations are the result of the 1–3 °C increase in temperature over most of East Asia (except Southeast China with cooling by ~1 °C) and changes in the atmospheric flow pattern. 2050 has enhanced Arctic transport from the stronger low pressure area over Eastern Russia, which leads to an increase of O_3 in the Arctic, especially Alaska and Western Canada. The 2050_CCO simulations show eastward and northward transport of the plume that is stronger than 2001 due to higher temperatures but weaker than 2050 due to lower O_3 precursor emissions. There is also an enhancement in Western Mexico, due to a combination of less water vapor which increases the lifetime of O_3 and greater subsidence of O_3 from the reduction in wind speeds aloft.

The vertical cross sections of O_3 show large differences between 850 mb and 400 mb for all simulations and the gradients are tilted toward the east, indicating that the O_3 is uplifted and carried eastward. A strong gradient exists near the surface from 120° E to 120° W, indicating a significant transport of O_3 in the PBL between East Asia and

ACPD
13, 26489–26527, 2013

Western North America. In 2050, greater generation of O_3 from increased precursor emissions and temperatures leads to greater lofting of O_3 into the FT and subsequently greater subsidence of O_3 downwind compared to 2001. In 2050_CCO, there is less lofting and thus less of a downwind impact on O_3 as compared to 2001. This results from increases in atmospheric stability, particularly from the surface to ~850 mb, that inhibits vertical transport. This indicates that future emission changes may overwhelm natural transport restrictions from climate change.

EAAEs also enhance the levels of other trace gases such as carbon monoxide (CO), sulfur dioxide (SO_2), and peroxyacetyl nitrate (PAN). EAAEs contribute ~13 ppb and ~16 ppb to the global average CO level under the current and future scenarios, respectively; the increase in 2050 mainly results from emission increases in Southeast Asia as the 2050_CCO simulations with and without EAAEs show only a slightly increased contribution (~14 ppb on global average) as compared to 2001. The impact of EAAEs is fairly uniform across the entire NH where they typically account for 5–10 and 10–30 ppb of the CO level in 2001 and 2050, respectively, but the impact is greater in immediate downwind regions such as North America, where the impact is 10–25 ppb in 2001 and 15–35 ppb in 2050. EAAEs-induced SO_2 has a weak transport signal as it accounts only for ~1–5 ppb in local areas of East China and Northeast India under current and future scenarios, but has a negligible contribution elsewhere. EAAEs contribute ~2 ppb SO_2 to the 24° N to 60° N meridional averaged surface concentrations with a decreased contribution of ~0.05 ppb up to ~450 mb between 75° E and 150° E and negligible contributions elsewhere. PAN exhibits a similar spatial distribution of contributions as O_3 since they share the same precursors. In 2001, EAAEs contribute ~0.04 ppb (0.2–1.0 ppb East Asia) to the global average PAN level and this nearly doubles to ~0.07 ppb (0.2–1.8 ppb in East Asia) in 2050 as a result of increased precursor emissions. The 2050 emission increase also generates contributions of 0.1–0.2 ppb to the PAN level over the majority of the NH compared to a more negligible contribution in 2001. The 24° N to 60° N meridional averaged vertical PAN contribution exhibits a similar trend. In 2001 EAAEs contribute ~0.3–0.5 ppb of PAN in East Asia between the

ACPD
13, 26489–26527, 2013

surface and 700 mb. The contribution is ~0.1–0.2 ppb over much of the North Pacific and portions of Western North America above 900 mb, indicating that there is transport aloft but the subsidence to the surface is negligible. In 2050, the contribution over East Asia increases to ~0.9–0.3 ppb from the surface to roughly 450 mb due to the increase in precursor emissions. The enhancement of PAN aloft leads to additional eastward transport with contributions of ~0.1–0.2 ppb at the surface in Western North America, Europe, and North Africa due to subsidence.

Figure 6 shows the differences in the 24 h averaged surface concentrations and the 24° N to 60° N meridional averaged vertical profiles of $PM_{2.5}$ with and without EAAEs for 2001, 2050, and 2050_CCO. The impact of EAAEs on $PM_{2.5}$ is not as homogeneous as the impact on some trace gases because its concentration and formation are more sensitive to changes in climate. On a global average, EAAEs account for 0.3–0.4 $\mu g\,m^{-3}$ in all scenarios with a slight increase from 0.32 in 2001 to 0.39 $\mu g\,m^{-3}$ in 2050 on a global average but larger increases in some regions (e.g., up to 3 $\mu g\,m^{-3}$ in the Pacific Ocean) (despite projected reductions in primary aerosol emissions in 2050), with most of the positive contributions over East Asia and the North Pacific. Over the interior of North America in all scenarios, EAAEs reduce the surface $PM_{2.5}$ level by 0.5–1.5 $\mu g\,m^{-3}$. This can be attributed to the increased PBLH generated by EAAEs in this region. The mechanism by which EAAEs can impact PBLH is discussed in greater detail in Sect. 6. A similar situation occurs over Scandinavia in the 2001 simulations, where EAAEs reduce the local $PM_{2.5}$ level (by ~0.5–3 $\mu g\,m^{-3}$). This impact is larger than that over North America due to the stagnant conditions over Scandinavia, during which vertical mixing becomes the strongest meteorological process impacting $PM_{2.5}$ (with wind speeds $< 1\,m\,s^{-1}$), but does not occur in 2050 or 2050_CCO due to the low pressure center that moves into this area in the future scenarios. Feedbacks from EAAEs to the 10 m wind speed (see Fig. 9) are distinctly different among all scenarios, which lead to differences in the concentrations of sea salt emitted in marine environments and concentrations of dust emitted over North Africa. This implies that such feedbacks are heavily dependent on both anthropogenic emissions and climate. The

ACPD
13, 26489–26527, 2013

contribution to the vertical distribution of $PM_{2.5}$ shows distinct difference between the impact in the PBL and lower FT, where the impact can be either an increase or a decrease, and that in the middle and upper free troposphere, where the impact is entirely an increase. This occurs because only stratiform cloud feedbacks are treated in this version of the model and these clouds are typically not present above ~500 mb. At this altitude, EAAEs increase the $PM_{2.5}$ level by 0.1–1.0 $\mu g\,m^{-3}$. This is why the impact on aerosol optical depth (AOD) (see Sect. 6) is almost entirely an increase over most of the NH despite the surface $PM_{2.5}$ impact being either positive or negative.

Figure 7 shows the contributions of EAAEs to surface BSOA and the total deposition fluxes of total nitrogen, black carbon, and mercury (TNTD, BCTD, and HgTD, respectively) (i.e., the differences in the surface BSOA, TNTD, BCTD, and HgTD between the simulations with and without EAAEs for 2001 and 2050). EAAEs demonstrate a strong impact on the BSOA in East Asia. EAAEs increase BSOA in East Asia by 0.1–1.2 $\mu g\,m^{-3}$ (10–81 %) with large areas experiencing an increase of 0.5–1.2 $\mu g\,m^{-3}$ (50–81 %) under all scenarios, indicating that a large fraction of BSOA in East Asia is controllable through controlling EAAEs that affect the oxidant levels for the oxidation of BSOA precursors. These results are consistent with the work of Carlton et al. (2010), who reported that over 50 % of the BSOA is controllable over the Southeastern US. However, further downwind EAAEs can decrease the amount of BSOA as they reduce incoming shortwave radiation fluxes at the Earth's surface (ISR), in turn decreasing the photolytic rate of NO_2 (JNO_2) and the amount of hydroxyl radical available to oxidize BSOA precursors.

EAAEs account for ~0.01–0.9 $g\,m^{-2}\,month^{-1}$ (40–98 %) of TNTD in East Asia and the North Pacific in 2001 and ~0.01–0.6 $g\,m^{-2}\,month^{-1}$ (20–97 %) in 2050. The decrease in 2050 is the result of a projected decrease in emissions of NH_3. This indicates that EAAEs are a contributor to the nitrogen fertilization of the Pacific Ocean and can enhance ocean productivity in areas that are nitrogen limited (Duce et al., 2008). Another key difference in 2050 is an increase of 0.001–0.002 $g\,m^{-2}\,month^{-1}$ (10–40 %) in TNTD over Alaska and other portions of the Arctic due to enhanced southerly trans-

ACPD
13, 26489–26527, 2013

port as compared to 2001. This enhanced Arctic deposition may help fertilize Arctic vegetation increasing their growth (Schindler and Bayley, 1993), thus potentially amplifying the climate feedbacks from enhanced shrub growth in that region (Chapin et al., 2005). EAAEs increase the global average BCTD by $\sim 3.0 \times 10^{-3}\,g\,m^{-2}\,month^{-1}$ under all scenarios. In all scenarios EAAEs increase Arctic BCTD by $\sim 1 \times 10^{-4}$–$8 \times 10^{-4}\,g\,m^{-2}\,month^{-1}$ (~10–80 %). This implies that EAAEs may be a leading contributor to enhanced melting of Arctic snowpack as BC lowers the snowpack albedo (Warren and Wiscombe, 1980; Clarke and Noone, 1985). Additionally, EAAEs contribute to BCTD in both the Tibetan Plateau (1×10^{-3}–$3 \times 10^{-2}\,g\,m^{-2}\,month^{-1}$ or 20–80 %) and mountainous regions of Western North America (1×10^{-3}–$1 \times 10^{-2}\,g\,m^{-2}\,month^{-1}$ or 10–40 %), which could impact the melting of snow that is an important reservoir of water for local populations (Hadley et al., 2010; Qian et al., 2011). EAAEs increase the global average HgTD by $\sim 2.0 \times 10^{-8}\,g\,m^{-2}\,month^{-1}$ (~48 %), with varying contributions in different regions (e.g., 40–98 % in East Asia and the North Pacific and 20–70 % in the Arctic). In particular, EAAEs increase HgTD in North America by 10–40 %. These results are consistent with the work of Seigneur et al. (2004) and Strode et al. (2008), who reported that Asian anthropogenic emissions contribute 5–36 % and 14 % to the Hg deposition in North America, respectively. The large contributions over all these regions imply that EAAEs-induced HgTD could be a large source of methylmercury, which is bioavailable and can accumulate in rice crops and aquatic life leading to human exposure (Zhang et al., 2010; Meng et al., 2011).

6 The impact of EAAEs on the climate system

EAAEs affect regional and global climate under all scenarios. Figure 8 shows the contributions of EAAEs to cloud condensation nuclei (CCN) at a supersaturation of 0.5 %, cloud droplet number concentration (CDNC), cloud optical thickness (COT), AOD, ISR, and JNO_2 between the simulations with and without EAAEs for 2001, 2050, and 2050_CCO. At a supersaturation of 0.5 %, EAAEs increase the global average col-

ACPD
13, 26489–26527, 2013

umn CCN by $\sim 3.2 \times 10^7$ cm^{-2} (9.5 %), $\sim 1.7 \times 10^7$ cm^{-2} (3.5 %), and $\sim 3.6 \times 10^7$ cm^{-2} (11.4 %), respectively, where the reduced contribution in 2050 can be attributed to lower aerosol concentrations which result from reductions in primary aerosol emissions. The impacts across all scenarios are the largest in East Asia (5×10^7–1.3×10^9 cm^{-2}), the North Pacific (5×10^7–1.2×10^9 cm^{-2}), and portions of North America (5×10^7–1.5×10^8 cm^{-2}). The column CCN can also be reduced by EAAEs, as much as $\sim -3.0 \times 10^8$ cm^{-2}, in regions including Western Asia, Europe, and Africa, as a result of decreased aerosol number. Such decreases may result from decreasing nucleation of new particles or slight increases in precipitation over portions of those regions. The general increase in CCN translates to domainwide increases of 8.3×10^4 cm^{-2} (11.5 %), 5.3×10^4 cm^{-2} (8.5 %), and 7.9×10^4 cm^{-2} (19.5 %) in CDNC in 2001, 2050, and 2050_CCO, respectively. CDNC also increases the most in East Asia (2.0×10^5–2.7×10^6 cm^{-2}), the North Pacific (2.0×10^5–1.0×10^6 cm^{-2}) and portions of North America (1×10^5–4×10^5 cm^{-2}) but there are certain regions, such as Mexico in 2050, where EAAEs can result in a sizeable decrease (1.0×10^5–3.0×10^5 cm^{-2}). These decreases are associated with decreases (2–6 g m^{-2}) in the cloud liquid water path (LWP). The greatest impact of EAAEs on CDNC occurs in areas with the greatest LWP. In East Asia, these areas include Southeast Asia and Northeast China. In 2050 and 2050_CCO, these areas of larger LWP migrate to the northeast and the impact on CDNC becomes stronger due to the stronger low pressure area over Eastern Russia.

EAAEs increase the global average COT by ~0.2 with larger increases of 0.5–4.5 in East Asia and its downwind areas in both 2001 and 2050, as shown in Fig. 8. In 2050, the impact on COT is spread more evenly over the North Pacific, while in 2001 the impact is concentrated in the vicinity of the Philippine Sea. This results from changes in the global distribution of cloud LWP between 2050 and 2001, where the LWP increases (by 2–18 g m^{-2}) in the northernmost portion of the Pacific and Alaska and also in the subtropical North Pacific, there is also a decrease (by 2 to 6 g m^{-2}) over the Philippine Sea which weakens the impact in that region. The 2050_CCO scenario experiences the largest impact on COT with a global average impact of 0.3 and a stronger impact

ACPD
13, 26489–26527, 2013

(2.0–4.0) over the Western North Pacific. This is due to the combination of a greater LWP in the 2050 climate and a greater number of particles to increase the CDNC using the 2001 emissions. Additionally, EAAEs-induced aerosols increase the global average AOD by ~0.02 but up to 0.5 in East Asia in all cases. In both 2050 and 2050_CCO, the impact on AOD is reduced in the Arctic as a result of the stronger zonal transport over East Asia, which reduces the meridional transport of particles.

The increase in COT and AOD reduce the ISR by ~2.8 $W m^{-2}$ in 2001, ~2.5 $W m^{-2}$ in 2050, and ~3.0 $W m^{-2}$ in 2050_CCO on global average. The reductions can be as large as 38.2 $W m^{-2}$ (18.3 %), 32.6 $W m^{-2}$ (17.8 %), and 41.8 $W m^{-2}$ (21.7 %), respectively, in East Asia and the North Pacific. Over East Asia, the changes in ISR follow the pattern of CDNC, because increases in CDNC increase COT and result in decreasing ISR. The reduced ISR also leads to a reduction in JNO_2 by $\sim 2.4 \times 10^{-3}$–2.8×10^{-3} min^{-1} on global average across all scenarios. The reductions can be larger than 5×10^{-3} min^{-1} over East Asia, the North Pacific, and North America, indicating that EAAEs reduce photochemistry over the majority of the NH. This primarily reduces the production rate of atomic oxygen gas (O), which then leads to a reduction in the rate of formation of O_3 and OH. The amount of O_3 is not significantly impacted as changes in precursor amounts and transport are more dominant; however, the OH level is reduced slightly by $\sim 1 \times 10^{-3}$ ppt on global average. This slight reduction in oxidants can reduce the production of condensable organic gases and lead to slight reductions in aerosols, such as BSOA, as mentioned previously.

These changes in cloud properties and radiation from EAAEs propagate through the atmosphere and alter the meteorology of the globe. Figure 9 shows the differences in 2 m temperature, PBLH, and 10 m wind speed between the simulations with and without EAAEs for 2001, 2050, and 2050_CCO. The aforementioned EAAEs-induced changes result in global cooling of ~0.05 °C in 2001, ~0.02 °C in 2050, and ~0.04 °C in 2050_CCO. In 2001, the temperatures decrease by 0.25–1 °C in East Asia over regions where COT increases, indicating that changes in ISR are the controlling force. In North America, the temperature decreases by −0.25–2 °C over Northwestern US and West-

ACPD
13, 26489–26527, 2013

ern Canada, but increases by 0.25–0.75 °C over Eastern Canada. Both of these regions experience decreased ISR from EAAEs, but the extra cloudiness over Eastern Canada enhances the downwelling of longwave radiation, leading to an average temperature increase. In 2050, the cooling over East Asia from EAAEs is about 0.25–0.75 °C and there is warming over Northeastern China of 0.25–1.25 °C again from greater downwelling of longwave radiation. Over North America the cooling is also about 0.25–1 °C, except over Alaska where stronger reductions in ISR decrease the temperature by 0.5–1.5 °C. It is important to note that changes in global 2 m temperature are not represented in marine environments as the configuration of GU-WRF/Chem simulations used in this work does not contain an ocean model component to simulate the response of sea surface temperatures to changes in radiation. In addition to the surface temperature over the ocean, humidity in the marine boundary layer and large scale pressure patterns which are controlled by sea surface temperatures will not be impacted by changes in chemistry since sea surface temperatures are static.

Despite their spatial and magnitude discrepancies, all the above impacts have similar trends under both the current and future scenarios with a few exceptions. PBLH is a good example of this exception, since there is no clear trend in the global average with and without EAAEs. In 2001 and 2050, the global average difference with and without EAAEs is a negligible increase of 0.03 m and decrease of 0.8 m, respectively, while the 2050_CCO simulation shows a more pronounced decrease of 2.5 m. The lack of a clear trend is most likely because PBLH is not only sensitive to changes in the atmosphere but also to the interactions with the underlying land and ocean surface. This sensitivity may also explain why there is no robust model trend in PBLH from climate change (Murazaki and Hess, 2006). However, despite the lack of a clear global trend, there are some stronger regional signals in East Asia, North America, and Scandinavia. The contributions of EAAEs to PBLH over East Asia and North America are complex but there is a general trend for decreases of 20–100 m that are spatially co-located with changes in CDNC and COT. The increases in CDNC increase COT, reducing the amount of ISR reaching the surface; this decreases the amount of energy that is ex-

ACPD
13, 26489–26527, 2013

changed between the atmosphere and the underlying surface and reduces either the sensible heat flux or the latent heat flux and thus reduces the average PBLH. The contribution of EAAEs to PBLH in Scandinavia is not consistent, with an increase of ∼10–70 m in 2001 and a decrease of ∼10–30 m in 2050. The pattern for 2050_CCO is even more complex with an increase over Norway and Sweden and decrease over Finland. The inconsistency in this region comes from changes in the flow pattern. Scandinavia lies on the boundary between the average cyclone over the North Atlantic and the average anticyclone over the Mediterranean Sea. These two surface features have different positions in the different scenarios and thus the meteorology of Scandinavia and the impact from EAAEs vary with their movement. In 2001, when Scandinavia experiences stagnant conditions from the average cyclone being further upwind, the increase in PBLH from EAAEs in this scenario has a strong impact and reduces the $PM_{2.5}$ level at the surface by ∼1–3 $\mu g\,m^{-3}$ (see Figs. 2 and 6). This implies that chemistry feedbacks to meteorology from emission reductions may have the opposite effect on air pollution (i.e., enhance pollution) in some locations under certain conditions. The impact of EAAEs on PR and 10 m wind speed varies with both emissions and climate scenario and since the differences between the current and future scenario are relatively small, no robust information can be gleaned.

7 Concluding remarks

EAAEs have a strong impact on climate, air quality, and potentially the ecosystems of not only East Asia but other regions downwind under both current and future climate and emission scenarios. This is especially true for the Arctic which, in addition to the aforementioned impacts, is expected to undergo many changes (e.g., amplified warming, sea ice retreat, and strong ocean acidification) by the latter half of the 21st century (Steinacher et al., 2009; Vavrus et al., 2012). The dominant impacts of EAAEs are to increase chemical concentrations (e.g., O_3, CO, PAN, $PM_{2.5}$), total deposition fluxes of chemical species (e.g., total nitrogen, BC, Hg), most cloud/optical variables (e.g., CCN,

ACPD
13, 26489–26527, 2013

CDNC, AOD, and COT) but decrease some radiation/photolysis variables (e.g., downward/net shortwave radiation and photolytic rate of NO_2). Controlling EAAEs can reduce not only the concentrations and depositions of anthropogenic-induced pollutants (by up to 100 %) but also BSOA (by 10–81 %). However, some aerosol-cloud feedbacks (e.g., changes in PBLH) may potentially compensate the improvements expected from emission reductions in some regions (e.g., Scandinavia in 2001).

The intercontinental transport of Asian pollution will likely play a more important role in the future due to enhanced eastward and northward transport, increased gaseous precursor emissions, and increased temperatures under the climate and emissions scenarios considered in this work. In particular, the O_3 and $PM_{2.5}$ concentrations caused by EAAEs in 2050 will increase by 0.8 ppb and 0.07 $\mu g\,m^{-3}$, respectively, on global average and by up to 3–12 ppb and 1–3 $\mu g\,m^{-3}$ over some regions. This demonstrates a need for the governments of involved countries to consider the complex interplays between air pollutants and climate to develop integrated emission control strategies for optimal air quality management and climate mitigation.

Supplementary material related to this article is available online at http://www.atmos-chem-phys-discuss.net/13/26489/2013/acpd-13-26489-2013-supplement.pdf.

Acknowledgements. This work is supported by United States Environmental Protection Agency Science to Achieve Results Program Grant no. R83337601 and the National Sciences Foundation (NSF)/United State Department of Agriculture Earth System Modeling Program Grant No. AGS-1049200 at NCSU and 2012-67003-30192 at the University of Chicago/ANL. Thanks are due to Mark Richardson at Caltech and William C. Skamarock at NCAR, for developing global WRF on which the GU-WRF/Chem is based; Louisa Emmons and Francis Vitt at NCAR for providing CAM4 and MOZART4 emissions. Thanks are also due to Shuai Zhu, a former post-D researcher at NCSU, for adding the deposition fluxes in the model output.

ACPD
13, 26489–26527, 2013

References

Anenberg, S. C., West, J. J., Fiore, A. M., Jaffe, D. A., Prather, M. J., Bergmann, D., Cuvelier, K., Dentener, F. J., Duncan, B. N., Gauss, M., Hess, P., Jonson, J. E., Lupu, A., Mackenzie, I. A., Marmer, E., Park, R. J., Sanderson, M. G., Schultz, M., Shindell, D. T., Szopa, S., Vivanco, M. G., Wild, O., and Zeng, G.: Intercontinental impacts of ozone pollution on human mortality, Environ. Sci. Technol., 43, 6482–6487, doi:10.1021/es900518z, 2009.

Bey, I., Jacob, D. J., Logan, A., and Yantosca, R. M.: Asian chemical outflow to the Pacific in spring: Origins, pathways, and budgets, J. Geophys. Res., 106, 23097–23113, doi:10.1029/2001JD000806, 2001.

Carlton, A. G., Pinder, R. W., Bhave, P. V., and Pouliot, G. A.: To what extent can biogenic SOA be controlled?, Environ. Sci. Technol., 44, 3376–3380, doi:10.1021/es903506b, 2010.

Chapin III, F. S., Sturm, M., Serreze, M. C., McFadden, J. P., Key, J. R., Lloyd, A. H., McGuire, A. D., Rupp, T. S., Lynch, A. H., Schimel, J. P., Beringer, J., Chapman, W. L., Epstein, H. E., Euskirchen, E. S., Hinzman, L. D., Jia, G., Ping, C.-L., Tape, K. D., Thompson, C. D. C., Walker, D. A., and Welker, J. M.: Role of land-surface changes in arctic summer warming, Science, 310, 657–660, doi:10.1126/science.1117368, 2005.

Clarke, A. D. and Noone, K. J.: Soot in the Arctic snowpack: a cause for perturbations in radiative transfer, Atmos. Environ., 19, 2045–2053, 1985.

Cooper, O. R., Forester, C., Parrish, D., Trainer, M., Dunlea, E., Ryerson, T., Hubler, G., Fehsenfeld, F., Nicks, D., Holloway, J., de Gouw, J., Warneke, C., Roberts, J. M., Flocke, F., and Moody, J.: A case study of transpacific warm conveyor belt transport: influence of merging airstreams on trace gas import to North America, J. Geophys. Res., 109, D23S08, doi:10.1029/2003JD003624, 2004.

Doherty, R. M., Wild, O., Shindell, D. T., Zeng, G., MacKenzie, I. A., Collins, W. J., Fiore, A. M., Stevenson, D. S., Dentener, F., Schultz, M. G., Hess, P., Derwent, R. G., and Keating, T. J.: Impacts of climate change on surface ozone and intercontinental ozone pollution: a multimodel study, J. Geophys. Res. Atmos., 118, 3744–3763, doi:10.1002/jgrd.50266, 2013.

Duce, R. A., LaRoche, J., Altieri, K., Arrigo, K. R., Baker, A. R., Capone, D. G., Cornell, S., Dentener, F., Galloway, J., Ganeshram, R. S., Geider, R. J., Jickells, T. Kuypers, M. M., Langlois, R., Liss, P. S., Liu, M., Middelburg, J. J., Moore, C. M., Nickovic, S., Oschlies, Pedersen, T., Prospero, J., Schlitzer, R., Seitzinger, S., Sorensen, L. L., Uematsu, M., Ulloa, O.,

ACPD
13, 26489–26527, 2013

Voss, M., Ward, B., and Zamora, L.: Impacts of atmospheric anthropogenic nitrogen on the open ocean, Science, 320, 893–897, doi:10.1126/science.1150369, 2008.
Fiore, A. M., Dentener, F. J., Wild, O., Cuvelier, C., Schultz, M. G., Hess, P., Textor, C., Schulz, M., Doherty, R. M., Horowitz, L. W., MacKenzie, I. A., Sanderson, M. G., Shindell, D. T., Stevenson, D. S., Szopa, S., Van Dingenen, R., Zeng, G., Atherton, C., Bergmann, D., Bey, I., Carmichael, G., Collins, W. J., Duncan, B. N., Faluvegi, G., Folberth, G., Gauss, M., Gong, S., Hauglustaine, D., Halloway, T., Isaksen, I. S. A., Jacob, D. J., Jonson, J. E., Kaminski, J. W., Keating, T. J., Lupu, A., Marmer, E., Montanaro, V., Park, R. J., Pitari, G., Pringle, K. J., Pyle, J. A., Schroeder, S., Vivanco, M. G., Wind, P., Wojcik, G., Wu, S., and Zuber, A.: Multimodel estimates of intercontinental source–receptor relationships for ozone pollution, J. Geophys. Res., 114, D04301, doi:10.1029/2008JD010816, 2009.
Gong, S. L., Barrie, L. A., and Blanchet, J.-P.: Modeling sea-salt aerosols in the atmosphere: 1. model development, J. Geophys. Res., 102, 3805–3818, 1997.
Guenther, A., Karl, T., Harley, P., Wiedinmyer, C., Palmer, P. I., and Geron, C.: Estimates of global terrestrial isoprene emissions using MEGAN (Model of Emissions of Gases and Aerosols from Nature), Atmos. Chem. Phys., 6, 3181–3210, doi:10.5194/acp-6-3181-2006, 2006.
Hadley, O. L., Ramanathan, V., Carmichael, G. R., Tang, Y., Corrigan, C. E, Roberts, G. C., and Mauger, G. S.: Trans-pacific transport of black carbon and fine aerosols ($D < 2.5$ mm) into North America, J. Geophys. Res., 112, D05309, doi:10.1029/2006JD007632, 2007.
Hadley, O. L., Corrigan, C. E., Kirchstetter, T. W., Cliff, S. S., and Ramanathan, V.: Measured black carbon deposition on the Sierra Nevada snow pack and implication for snow pack retreat, Atmos. Chem. Phys., 10, 7505–7513, doi:10.5194/acp-10-7505-2010, 2010.
Hess, P. G. and Vukicevic, T.: Intercontinental transport, chemical transformations, and baroclinic systems, J. Geophys. Res., 108, 4354, doi:10.1029/2002JD002798, 2003.
Husar, R. B., Tratt, D. M., Schichtel, B. A., Falke, S. R., Li, F., Jaffe, D., Gasso, S., Gill, T., Laulainen, N. S., Lu, F., Reheis, M. C., Chun, Y., Westphal, D., Holben, B. N., Gueymard, C., McKendry, I., Kuring, N., Feldman, G. C., McClain, C., Frouin, R. J., Merrill, J., DuBois, D., Vignola, F., Murayama, T., Nickovic, S., Wilson, W. E., Sassen, K., Sugimoto, N., and Malm, W. C.: Asian dust events of April 1998, J. Geophys. Res., 106, 18317–18330, doi:10.1029/2000JD900788, 2001.
Jacob, D. J., Logan, J. A., and Murti, P. P.: Effect of rising Asian emission on surface ozone in the United States, Geophys. Res. Lett., 26, 2175–2178, doi:10.1029/1999GL900450, 1999.

ACPD
13, 26489–26527, 2013

Jaffe, D. A., Anderson, T., Covert, D., Kotchenruther, R., Trost, B., Danielson, J., Simpson, W., Berntsen, T., Karlsdottir, S., Blake, D., Harris, J., Carmichael, G., and Uno, I.: Transport of Asian air pollution to North America, Geophys. Res. Lett., 26, 711–714, doi:10.1029/1999GL900100, 1999.

Jaffe, D. A., McKendry, I., Anderson, T., and Price, H.: Six "new" episodes of trans-Pacific transport of air pollutants, Atmos. Environ., 37, 391–404, doi:10.1016/S1352-2310(02)00862-2, 2003.

Jonson, J. E., Stohl, A., Fiore, A. M., Hess, P., Szopa, S., Wild, O., Zeng, G., Dentener, F. J., Lupu, A., Schultz, M. G., Duncan, B. N., Sudo, K., Wind, P., Schulz, M., Marmer, E., Cuvelier, C., Keating, T., Zuber, A., Valdebenito, A., Dorokhov, V., De Backer, H., Davies, J., Chen, G. H., Johnson, B., Tarasick, D. W., Stübi, R., Newchurch, M. J., von der Gathen, P., Steinbrecht, W., and Claude, H.: A multi-model analysis of vertical ozone profiles, Atmos. Chem. Phys., 10, 5759–5783, doi:10.5194/acp-10-5759-2010, 2010.

Lau, K.-M. and Kim, K.-M.: Observational relationships between aerosol and Asian monsoon rainfall, and circulation, Geophys. Res. Lett., 33, L21810, doi:10.1029/2006GL027546, 2006a.

Lau, K. M., Kim, M. K., and Kim, K. M.: Asian monsoon anomalies induced by aerosol direct effects, Clim. Dynam., 26, 855–864, doi:10.1007/s00382-006-0114-z, 2006b.

Leibensperger, E. M., Mickley, L. J., Jacob, D. J., and Barrett, S. R. H.: Intercontinental influence of NO_x and CO on particulate matter air quality, Atmos. Environ., 45, 3318–3324, doi:10.1016/j.atmosenv.2011.02.023, 2011.

Lin, J.-T., Wuebbles, J. T., and Liang, X.-Z.: Effects of intercontinental transport on surface ozone over the US: present and future assessment with a global model, Geophys. Res. Lett., 35, L02805, doi:10.1029/2007GL031415, 2008.

Liu, H., Jacob, D. J., Bey, I., Yantosca, R. M., Duncan, B. N., and Sachse, G. W.: Transport pathways for Asian pollution outflow over the Pacific: interannual and seasonal variations, J. Geophys. Res., 108, 8786, doi:10.1029/2002JD003102, 2003.

Liu, J., Mauzerall, D. L., and Horowitz, L. W.: Source-receptor relationships between East Asian sulfur dioxide emissions and Northern Hemisphere sulfate concentrations, Atmos. Chem. Phys., 8, 3721–3733, doi:10.5194/acp-8-3721-2008, 2008.

Liu, J., Mauzerall, D. L., and Horowitz, L. W.: Evaluating inter-continental transport of fine aerosol 2) global health impact, Atmos. Environ., 43, 4339–4347, doi:10.1016/j.atmosenv.2009.05.032, 2009.

ACPD
13, 26489–26527, 2013

Masui, T. K., Hijioka, Y., Kinoshita, T., Nozawa, T., Ishiwatari, S., Kato, E., Shukla, P. R., Yamaga, Y., and Kainuma, M.: An emission pathway for stabilization at 6 Wm^{-2} radiative forcing, Climatic Change, 109, 59–76, doi:10.1007/s10584-011-0150-5, 2011.

Meng, B., Feng, X., Qiu, G., Liang, P., Li, P, Chen, C., and Shang, L.: The process of methylmercury accumulation in rice (*Oryza sativa* L.), Environ. Sci. Technol., 45, 2711–2717, doi:10.1021/es103384v, 2011.

Menon, S., Hansen, J., Nazarenko, L., and Luo, Y.: Climate effects of black carbon aerosols in India and China, Science, 297, 2250–2253, doi:10.1126/science.1075159, 2002.

Murazaki, K. and Hess, P.: How does climate change contribute to surface ozone change over the US?, J. Geophys. Res., 111, D05301, doi:10.1029/2005JD005873, 2006.

Nakicenovic, N., Davidson, O., Davis, G., Grubler, A., Kram, T., La Rovere, E. L., Metz, B., Morita, T., Pepper, W., Pitcher, H., Sankovski, A., Shukla, P., Swart, R., Watson, R., and Dadi, Z.: Emissions Scenarios: A Special Report of Working Group III of the Intergovernmental Panel on Climate Change, Cambridge University Press, New York, 2001.

O'Dowd, C., Smith, M. H., Consterdine, J. E., and Lowe, J. A.: Marine aerosol, sea-salt, and the marine sulphur cycle: a short review, Atmos. Environ., 31, 73–80, 1997.

Park, R. J., Jacob, D. J., Field, B. D., Yantosca, R. M., and Chin, M.: Natural and transboundary pollution influences on sulfate-nitrate-ammonium aerosols in the US: implications for policy, J. Geophys. Res., 109, D15204, doi:10.1029/2003JD004473, 2004.

Pfister, G. G., Emmons, L. K., Hess, P. G., Lamarque, J.-F., Thompson, A. M., and Yorks, J. E.: Analysis of the summer 2004 ozone budget over the US using Intercontinental Transport Experiment Ozonesonde Network Study (IONS) observations and Model of Ozone and Related Tracers (MOZART-4) simulations, J. Geophys. Res., 113, D23306, doi:10.1029/2008JD010190, 2008.

Qian, Y., Leung, L. R., Ghan, S. J., and Giorgi, F.: Regional climate effects of aerosols over China: modeling and observation, Tellus B, 55, 914–934, 2003.

Qian, Y., Kaiser, D. P., Leung, L. R., and Xu, M.: More frequent cloud-free sky and less surface solar radiation in China from 1955 to 2000, Geophys. Res. Lett., 33, L01812, doi:10.1029/2005GL024586, 2006.

Qian, Y., Wang, W., Leung, L. R., and Kaiser, D. P.: Variability of solar radiation under cloud-free skies in China: the role of aerosols, Geophys. Res. Lett., 34, L12804, doi:10.1029/2006GL028800, 2007.

ACPD
13, 26489–26527, 2013

Qian, Y., Flanner, M. G., Leung, L. R., and Wang, W.: Sensitivity studies on the impacts of Tibetan Plateau snowpack pollution on the Asian hydrological cycle and monsoon climate, Atmos. Chem. Phys., 11, 1929–1948, doi:10.5194/acp-11-1929-2011, 2011.

Ravetta, F., Ancellet, G., Colette, A., and Schlager, H.: Long-range transport and tropospheric ozone variability in the Western Mediterranean region during the Intercontinental Transport of Ozone and Precursors (ITOP-2004) campaign, J. Geophys. Res., 112, D10S46, doi:10.1029/2006JD007724, 2007.

Reidmiller, D. R., Fiore, A. M., Jaffe, D. A., Bergmann, D., Cuvelier, C., Dentener, F. J., Duncan, B. N., Folberth, G., Gauss, M., Gong, S., Hess, P., Jonson, J. E., Keating, T., Lupu, A., Marmer, E., Park, R., Schultz, M. G., Shindell, D. T., Szopa, S., Vivanco, M. G., Wild, O., and Zuber, A.: The influence of foreign vs. North American emissions on surface ozone in the US, Atmos. Chem. Phys., 9, 5027–5042, doi:10.5194/acp-9-5027-2009, 2009.

Riahi, K., Rao, S., Krey, V., Cho, C., Chirkov, V., Fischer, G., Kindermann, G., Nakicenovic, N., and Rafaj, P.: RCP 8.5-A scenario of comparatively high greenhouse gas emissions, Climatic Change, 109, 33–57, doi:10.1007/s10584-011-0149-y, 2011.

RIVM (National Institute for Public Health and the Environment): The IMAGE 2.2 Implementation of the SRES Scenarios [CD-ROM], RIVM Publication 481508018, Bilthoven, Netherlands, 2001.

Roberts, G., Mauger, G., Hadley, O., and Ramanathan, V.: North American and Asian aerosols over the Eastern Pacific Ocean and their role in regulating cloud condensation nuclei, J. Geophys. Res., 111, D13205, doi:10.1029/2005JD006661, 2006.

Sanderson, M. G., Dentener, F. J., Fiore, A. M., Cuvelier, C., Keating, T. J., Zuber, A., Atherton, C. S., Bergmann, D. J., Diehl, T., Doherty, R. M., Duncan, B. N., Hess, P., Horowitz, L. W., Jacob, D. J., Jonson, J.-E., Kaminski, J. W., Lupu, A., MacKenzie, I. A., Mancini, E., Marmer, E., Park, R., Pitari, G., Prather, M. J., Pringle, K. J., Schroeder, S., Schultz, M. G., Shindell, D. T., Szopa, S., Wild, O., and Wind, P.: A multi-model study of the hemispheric transport and deposition of oxidised nitrogen, Geophys. Res. Lett., 35, L17815, doi:10.1029/2008GL035389, 2008.

Schindler, D. W. and Bayley, S. E.: The biosphere as an increasing sink for atmospheric carbon: estimates from increased nitrogen deposition, Global Biogeochem. Cy., 7, 717–733, 1993.

Seigneur, C., Vijayaraghavan, K., Lohman, K., Karamchandani, P., and Scott, C.: Global source attribution for mercury deposition in the US, Environ. Sci. Technol., 28, 555–569, doi:10.1021/es034109t, 2004.

ACPD
13, 26489–26527, 2013

Shaw, P.: Application of aerosol speciation data as an in situ dust proxy for validation of the Dust Regional Atmospheric Model (DREAM), Atmos. Environ., 42, 7304–7309, doi:10.1016/j.atmosenv.2008.06.018, 2008.

Shindell, D. T., Chin, M., Dentener, F., Doherty, R. M., Faluvegi, G., Fiore, A. M., Hess, P., Koch, D. M., MacKenzie, I. A., Sanderson, M. G., Schultz, M. G., Schulz, M., Stevenson, D. S., Teich, H., Textor, C., Wild, O., Bergmann, D. J., Bey, I., Bian, H., Cuvelier, C., Duncan, B. N., Folberth, G., Horowitz, L. W., Jonson, J., Kaminski, J. W., Marmer, E., Park, R., Pringle, K. J., Schroeder, S., Szopa, S., Takemura, T., Zeng, G., Keating, T. J., and Zuber, A.: A multi-model assessment of pollution transport to the Arctic, Atmos. Chem. Phys., 8, 5353–5372, doi:10.5194/acp-8-5353-2008, 2008.

Steinacher, M., Joos, F., Frölicher, T. L., Plattner, G.-K., and Doney, S. C.: Imminent ocean acidification in the Arctic projected with the NCAR global coupled carbon cycle-climate model, Biogeosciences, 6, 515–533, doi:10.5194/bg-6-515-2009, 2009.

Stohl, A., Eckhardt, S., Forster, C., James, P., and Spichtinger, N.: On the pathways and timescales of intercontinental air pollution transport, J. Geophys. Res., 107, 4684, doi:10.1029/2001JD001396, 2002.

Strode, S. A., Jaegle, L., Jaffe, D. A., Swartzendruber, P. C., Selin, N. E., Holmes, C., and Yantosca, R. M.: Trans-Pacific transport of mercury, J. Geophys. Res., 113, D15305, doi:10.1029/2007JD009428, 2008.

Sudo, K. and Akimoto, H.: Global source attribution of tropospheric ozone: long-range transport from various source regions, J. Geophys. Res., 112, D12302, doi:10.1029/2006JD007992, 2007.

Takigawa, M., Sudo, K., Akimoto, H., Kita, K., Takegawa, N., Kondo, Y., and Takahashi, M.: Estimation of the contribution of intercontinental transport during the PEACE campaign by using a global model, J. Geophys. Res., 110, D21313, doi:10.1029/2005JD006226, 2005.

TF HTAP – Task Force on Hemispheric Transport of Air Pollution: Hemispheric Transport of Air Pollution 2010, Part A: Ozone and Particulate Matter, Air Pollut. Stud., 17, edited by: Dentener, F., Keating, T. J., and Akimoto, H., United Nations Economic Commission for Europe, Geneva, Switzerland, available at: http://www.htap.org (last access: August 2013), 2011.

Vavrus, S. J., Holland, M. M., Jahn, A., Bailey, D. A., and Blazey, B. A.: Twenty-first-century arctic climate change in CCSM4, J. Climate, 25, 2696–2710, doi:10.1175/JCLI-D-11-00220.1, 2011.

ACPD
13, 26489–26527, 2013

Wang, K., Zhang, Y., Jang, C., Phillips, S., and Wang, B.: Modeling intercontinental air pollution transport over the trans-Pacific region in 2001 using the community multiscale air quality modeling system, J. Geophys. Res., 114, D04307, doi:10.1029/2008JD010807, 2009.

Wang, K., Zhang, Y., Nenes, A., and Fountoukis, C.: Implementation of dust emission and chemistry into the Community Multiscale Air Quality modeling system and initial application to an Asian dust storm episode, Atmos. Chem. Phys., 12, 10209–10237, doi:10.5194/acp-12-10209-2012, 2012.

Warren, S. G. and Wiscombe, W. J.: A model for the spectral albedo of snow. II: Snow containing atmospheric aerosols, J. Atmos. Sci., 37, 2734–2745, 1980.

Wild, O. and Akimoto, H.: Intercontinental transport of ozone and its precursors in a three-dimensional CTM, J. Geophys. Res., 106, 27729–27744, 2001.

Yu, H., Remer, L. A., Chin, M., Bian, H., Kleidman, R. G., and Diehl, T.: A satellite-based assessment of transpacific transport of pollution aerosol, J. Geophys. Res., 113, D14S12, doi:10.1029/2007JD009349, 2008.

Zhang, H., Feng, X., Larssen, T., Qiu, G., and Vogt, R. D.: In inland China, rice, rather than fish, is the major pathway for methylmercury exposure, Environ. Health Persp., 118, 1183–1188, 2010.

Zhang, L., Jacob, D. J., Boersma, K. F., Jaffe, D. A., Olson, J. R., Bowman, K. W., Worden, J. R., Thompson, A. M., Avery, M. A., Cohen, R. C., Dibb, J. E., Flock, F. M., Fuelberg, H. E., Huey, L. G., McMillan, W. W., Singh, H. B., and Weinheimer, A. J.: Transpacific transport of ozone pollution and the effect of recent Asian emission increases on air quality in North America: an integrated analysis using satellite, aircraft, ozonesonde, and surface observations, Atmos. Chem. Phys., 8, 6117–6136, doi:10.5194/acp-8-6117-2008, 2008.

Zhang, R., Li, G., Fan, J., Wu, D. L., and Molina, M. J.: Intensification of Pacific storm track linked to Asian pollution, P. Natl. Acad. Sci. USA, 104, 5295–5299, 2007.

Zhang, Y., Hemperly, J., Meskhidze, N., and Skamarock, W. C.: The Global Weather Research and Forecasting (GWRF) model: model evaluation, sensitivity study, and future year simulation, Atmospheric and Climate Sciences, 2, 231–253, doi:10.4236/acs.2012.23024, 2012a.

Zhang, Y., Karamchandani, P., Glotfelty, T., Streets, D. G., Grell, G., Nenes, A., Yu, F., and Bennartz, R.: Development and initial application of the global-through-urban weather research and forecasting model with chemistry (GU-WRF/Chem), J. Geophys. Res., 117, D20206, doi:10.1029/2012JD017966, 2012b.

ACPD
13, 26489–26527, 2013

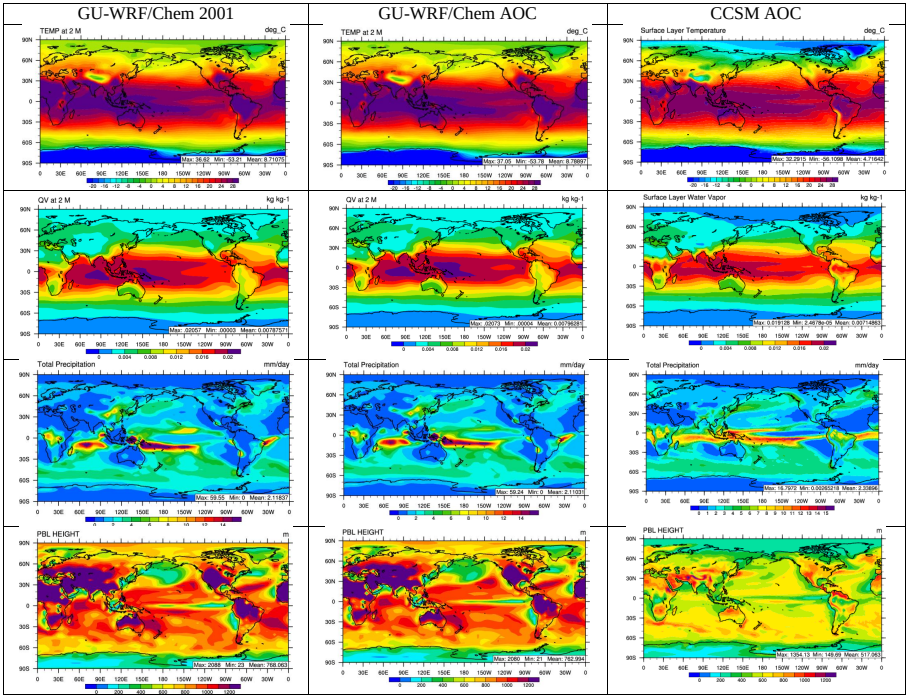

Fig. 1. Average spring (MAM) 2 m temperature, 2 m water vapor, precipitation rate, and planetary boundary layer height fields from GU-WRF/Chem simulations of the year 2001 (left), averaged current period consisting of 2001 and 2010 (AOC) (center), and the average of the current period 2000–2014 from CCSM3 initial conditions (right).

ACPD
13, 26489–26527, 2013

Will the role of intercontinental transport change in a changing climate?

T. Glotfelty et al.

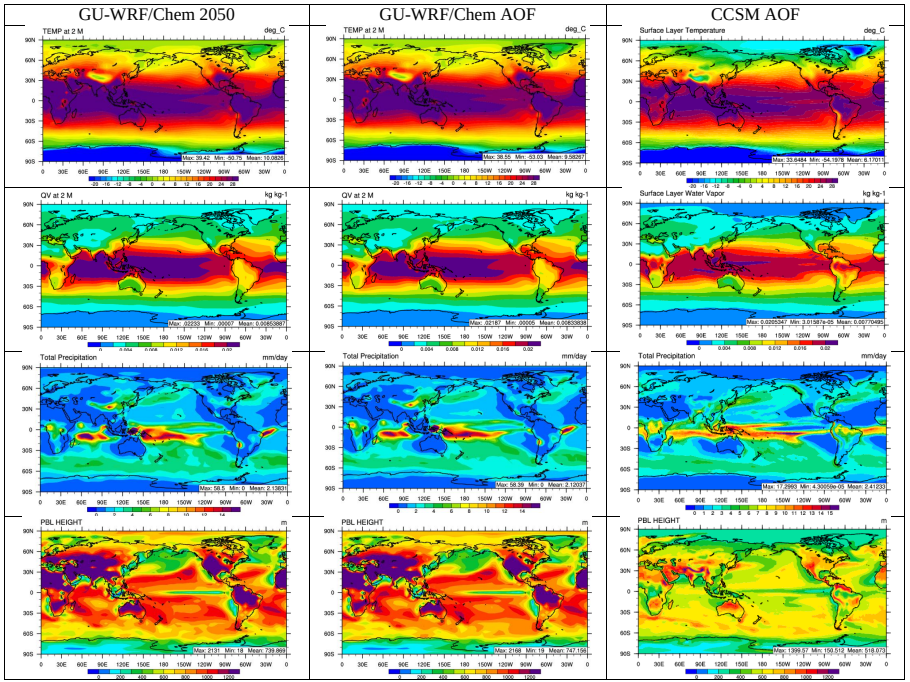

Fig. 2. Average spring (MAM) 2 m temperature, 2 m water vapor, precipitation rate, and planetary boundary layer height fields from GU-WRF/Chem simulations of the year 2050 (left), averaged future period consisting of 2020, 2030, 2040, and 2050 (AOF) (center), and the average of the future period 2015–2054 from CCSM3 initial conditions (right).

ACPD
13, 26489–26527, 2013

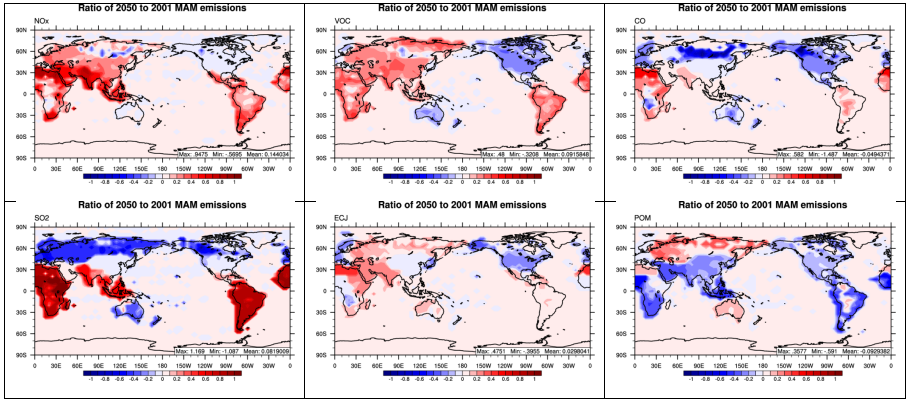

Fig. 3. The logarithm of the ratio of 2050 spring (MAM) emissions to the 2001 MAM emissions of NO_x, total non-methane VOC, CO, SO_2, black carbon, and primary organic carbon.

ACPD
13, 26489–26527, 2013

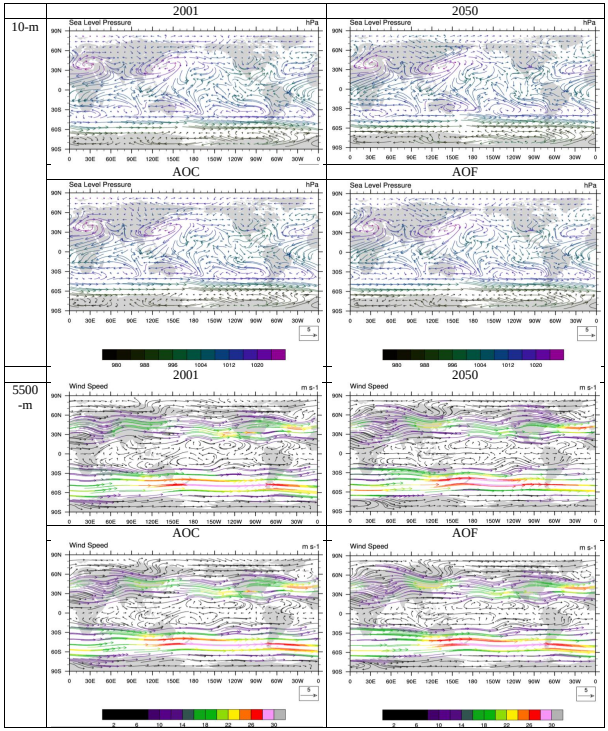

Fig. 4. The average spring (MAM) weather patterns at the surface (top) and 5500 m (bottom) for 2001 and the average current period (left), 2050 and the average future period (right) from the baseline simulations. The surface plots depict the wind vectors from the 10 m wind components and the color scale is based on the sea level pressure. The 5500 m vectors are derived from the wind components interpolated to that height and the color scale is the magnitude of the wind speed.

ACPD
13, 26489–26527, 2013

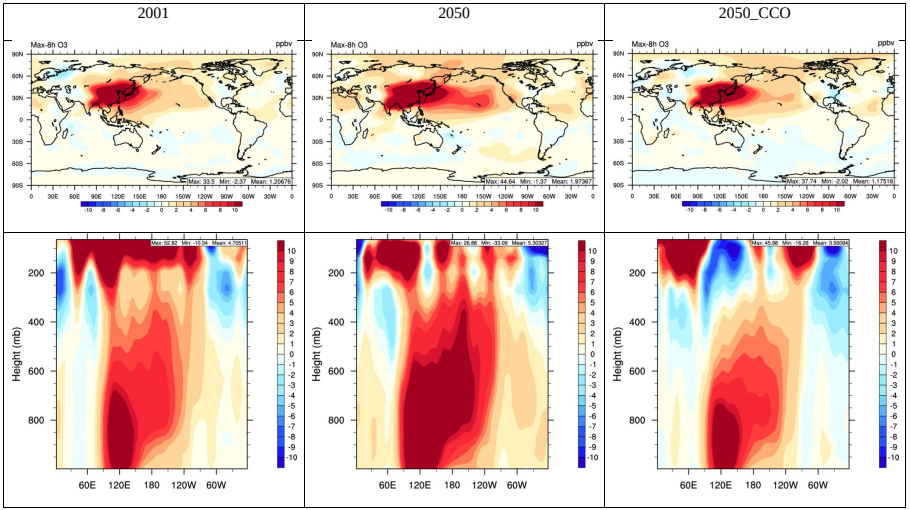

Fig. 5. The difference in the spring (MAM) maximum 8 h average surface ozone mixing ratio (top) and the mid-latitude (24° N to 60° N) meridional averaged vertical cross section of ozone (bottom) between the simulations with and without EAAEs for the current (2001) and future (2050 and 2050_CCO) scenarios.

ACPD
13, 26489–26527, 2013

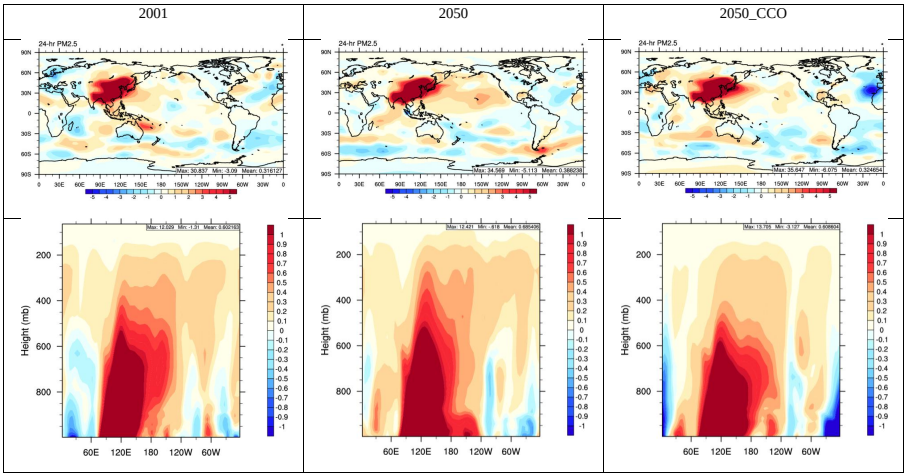

Fig. 6. The difference in the spring (MAM) 24 h average $PM_{2.5}$ concentration (top) and the mid-latitude (24° N to 60° N) meridional averaged vertical cross section of $PM_{2.5}$ (bottom) between the simulations with and without EAAEs for the current (2001) and future (2050 and 2050_CCO) scenarios.

ACPD
13, 26489–26527, 2013

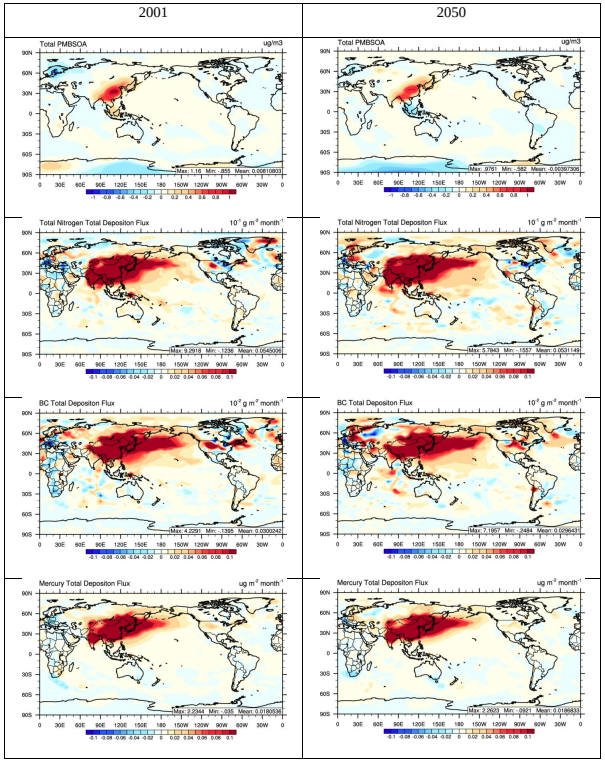

Fig. 7. The difference in the spring (MAM) BSOA concentration (row 1), total deposition of total nitrogen (row 2), black carbon aerosol (row 3), and total gaseous and particulate mercury (row 4) between the simulations with and without EAAEs for the current (2001) and future (2050) scenarios.

ACPD
13, 26489–26527, 2013

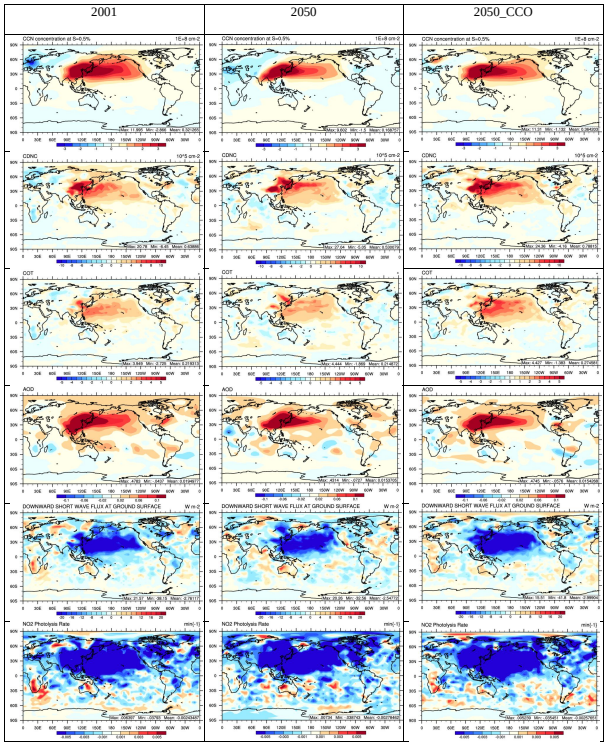

Fig. 8. The difference in the spring (MAM) average cloud condensation nuclei (CCN), cloud droplet number concentration (CDNC), cloud optical thickness (COT), aerosol optical depth (AOD), downward solar radiation flux (ISR), and the photolysis rate of NO_2 (JNO_2) between the simulations with and without EAAEs for the current (2001), future (2050), and climate change only (2050_CCO) scenarios.

ACPD
13, 26489–26527, 2013

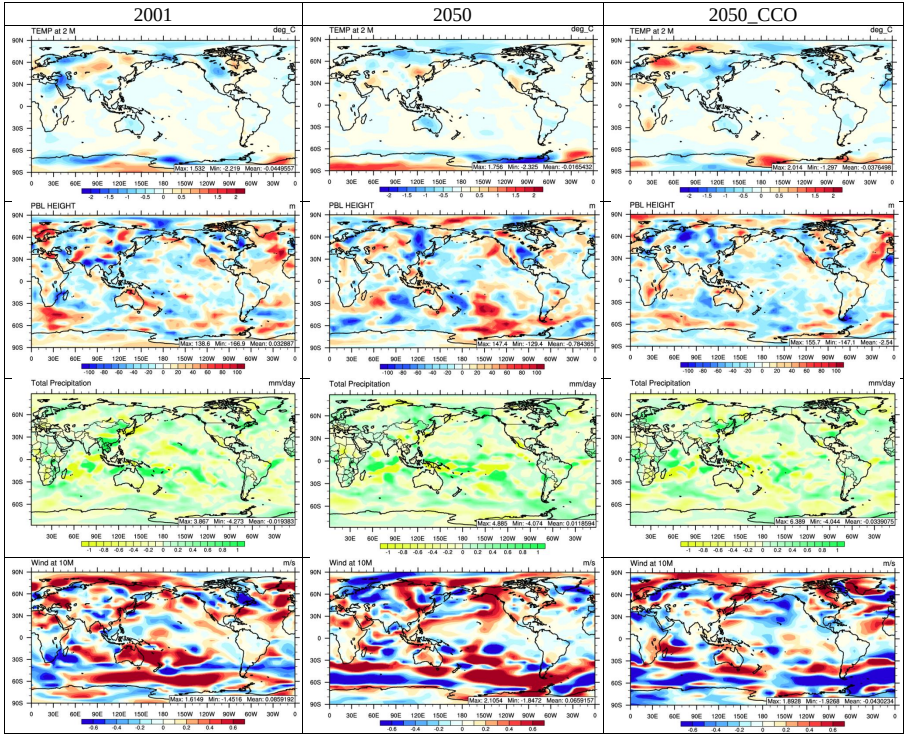

Fig. 9. The difference in the spring (MAM) average 2 m temperature, planetary boundary layer height, total precipitation rate, and 10 m wind speed between the simulations with and without EAAEs for current (2001), future (2050), and climate change only (2050_CCO).

ACPD
13, 26489–26527, 2013